Two-dimensional measurement of natural radioactivity of some Archean and Proterozoic rocks from South Africa

Noriyoshi Tsuchiya and Mihoko Hareyama

Department of Geoscience and Technology, Tohoku University,
Aoba-ku, Aoba 01, Sendai 980-8579

Abstract: The imaging plate is employed as a radiation sensor for obtaining two-dimensional radiation images of natural radioactivity. We used it to evaluate the autoradiography of several types of Archean and Proterozoic granitoids and ultramafic rocks from South Africa for obtaining the distribution of radiation emitters. The semi-quantitative dose of natural radioactivity, represented by PSL value in the imaging plate measuring system (the intensity of photostimulated luminescence per unit area), is shown in terms of the potassium content. Both beta and gamma ray doses were estimated on the basis of functional relationship between potassium content and respective PSL values. Comparing Japanese granitoids analyzed in this study, Archean and Proterozoic granitoids from South Africa used here show relatively high radiation effects caused by disintegration of uranium, thorium and actinium decay series.

key words: natural radioactivity, imaging plate, South Africa, Archean, Proterozoic

1. Introduction

The imaging plate is a storage film, coated with radiation-sensitive photostimulated phosphor ($BaFBr:Eu^{2+}$), and widely used in a variety of geological fields (Momoshima *et al.*, 1995; Tsuchiya *et al.*, 1998; Hareyama *et al.*, 1998, 2000). Latent images produced by irradiation of the imaging plate are read by superficial scanning with stimulation light and are reconstructed as two-dimensional dot images. The imaging plate is an efficient radiation detector, with several advantageous attributes, including ease of use, high position resolution, large detection area, high detection sensitivity with high signal-to-noise ratio, extended time dose accumulation, dose linearity, an extremely wide dose dynamic range, and an erasing capability for reuse. The physical mechanism of photostimulated luminescence for the radiation effect has been well investigated (Takahashi *et al.*, 1984; Thomas *et al.*, 1991; Iwabuchi *et al.*, 1994; Takebe and Abe, 1994; Takebe *et al.*, 1995), and Hareyama *et al.* (2000) recently summarized the energy term scheme of photostimulated luminescence.

Hareyama *et al.* (2000) described irradiation images of Cretaceous granitic rocks in Japan, and showed that a functional relationship existed between semi-quantitative dose rate and potassium content. Rocks have potassium, uranium, thorium, and rubidium as radioactive elements, but natural radioactivity can be estimated mainly from the potassium content, because ^{40}K is the major radioactive isotope in natural rocks.

167

Early Archean granitoids, as well as other Proterozoic rocks, were collected during a geological expedition to South Africa in 1997 and 1998. This study describes high quality two-dimensional natural irradiation patterns for some South African plutonics and orthogneiss, captured with the imaging plate, and makes comparisons with a semi-quantitative determination of natural radioactivity based on whole rock potassium content.

2. Geological outline and sample description

Figure 1 shows a simplified geological map of eastern South Africa, and sample localities for rocks collected in this study. The samples were collected from Archean sequences in the Barberton Greenstone Belt, the Limpopo Belt and the Natal metamorphic province, which covers a large geological time scale (from Early Archean at ~3500 Ma, to middle Proterozoic at ~1000 Ma). The geological outline for each area, and sample descriptions, are as follows:

978080703A-1: Charnockite. This megacrystic and charnockitic is a part of the Port Edward Pluton which is a member of the Oribi Gorge Suite in the Natal Belt. The charnockite is characterized by megacrystic feldspar (plagioclase+K-feldspar). Interstitial to the feldspar are the mafic minerals (mostly orthopyroxene, lesser clinopyroxene, locally hornblende and biotite) and quartz. Also concentrated in the interstices are apatite and zircon which occur as poikilitic inclusions in the mafic minerals. A Rb-Sr whole rock age, given by Grantham and Eglington (1992), is 987±19 Ma.

97080806B: Rapakivi granite. The coarse-grained (up to 2 cm in diameter), porphyritic rapakivi granite comprises part of the Oribi Gorge Suite, in the Natal Belt. K-feldspar phenocrysts, which are deformed, are mantled with plagioclase. The age of this sample is inferred to be similar to 97080703A-1 (*i.e.* ~1000 Ma).

97081509A: Granite. The Limpopo Belt has been subdivided into three zones: Northern Marginal Zone (NMZ), Central Zone (CZ) and Southern Marginal Zone (SMZ), after Watkeys (1983) and McCourt (1986). The southern limit of the SMZ is represented by a shear zone, whereby the granulite terrane of the Limpopo Belt is believed to have been thrust northward onto the Zimbabwe Craton in the north, and southward onto the Kaapvaal Craton in the south (Van Reenen *et al.*, 1987). The Matok complex, which straddles the orthopyroxene isograd midway between the towns of Pietersburg and Luis Trichardt, represents a differentiated pluton, with a mafic granodioritic facies grading into a porphyritic granite facies and leucocratic late-stage granite. Analysis of samples from the porphyritic granite yields a Rb-Sr isochron age of 2620±75 Ma. Additional geochronological data indicate 2670 Ma, which is comparable to the so-called '2650 Ma granite' (Barton *et al.*, 1983a: Roering *et al.*, 1992).

97082002 series: Dunite. Rocks of the Early Archean greenstone-granite terrane characterize the Barberton Mountain Land. Here, the Swaziland Supergroup of the Barberton Greenstone Belt has a tripartite stratigraphy, with the lower volcanic succession (Onverwacht Group) overlain by two sedimentary successions (Fig Tree, and Moodies Groups, respectively), (Anhaeusser *et al.*, 1983; Windley, 1996).

In the Eastern Transvaal and Swaziland, volcano-sedimentary assemblages of the Onverwacht, Fig Tree and Moodies Groups constitute the Barberton Sequences. Three
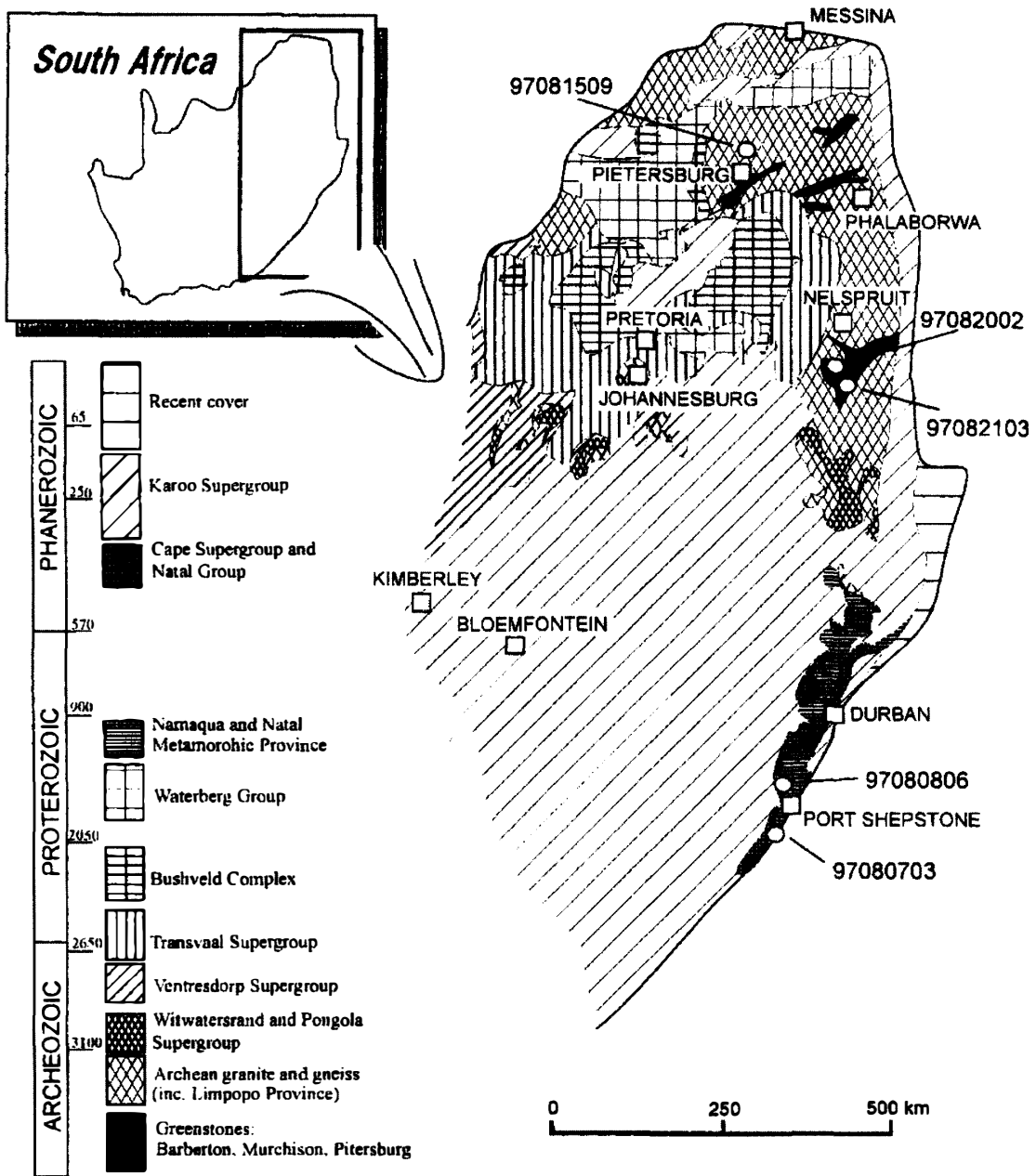
Fig. 1. Simplified geological map of South Africa and sample localities.

formations, Sandspuruit, Theespruit, and Komati Formations, make up the Tjakastad Subgroup at the base of the succession. These sequences are also known as the Lower Ultramafic Unit, with the lower formation being dominated by mafic and ultramafic lavas (predominantly komatiites and basaltic komatiites), together with subordinate amounts of felsic tuff and agglomerate, banded chert, banded iron-formation, calc-silicate rocks and soda-rich porphyry bodies. The ultramafic intrusive complexes contain serpentinized dunite, harzburgite and orthopyroxenite, with lesser amounts of clinopyroxenite, gabbro and anorthosite, as penecontemporaneous sill-like bodies, associated with the komatiitic extrusive sequences.

To the north of Barberton, a narrow tract of country, referred to as the Jamestown Schist Belt (Anhaeusser, 1972), forms a wedge between the Kaap Valley Granite to the south and Nelspruit gneisses and migmatites to the north. The Jamestown Schist Belt is almost entirely composed of Archean (~3400 Ma) rocks of the Onverwacht Group. The south-western extremity and the south-eastern portion of the Schist Belt consist almost entirely of mafic and ultramafic rocks of a massive and schistose habit. The intrusive assemblages grade into a succession of layered differentiated ultramafic bodies, comprising a number of cyclic units of dunite, peridotite, pyroxenite, and gabbro.

Figure 2 shows two-dimensional compositional mapping of Si and Mn for 97082002B, obtained by X-ray analytical microscope. The 97082002 sample series comprise weakly serpentinized dunite, with rhodochrosite and magnesite phenocryst phases. Experimental conditions for compositional mapping are described in a later section.

97082103A-1: Trondhjemitic gneiss. Hornblende tonalite and leucocratic biotite trodhjemite underlie large areas of the Archean granitic terrane, with several discrete tonalite-trondhjemite bodies having been identified west and south-west of the Barberton Greenstone Belt. Robb and Anhaesser (1983) subdivided those tonalite and trondhjemite intrusives, each representing an individual magmatic event, into 13 spatially and temporally unrelated plutons and cells. According to their definition, 97082103A-1 may be classified into the Theeboom Cell, which has been recognized by several workers as being part of the Stolzburg Pluton. The foliated trodhjemite gneiss occurs with a set of remnant linear amphibolite dikes, of basaltic komatiitic composition, which are inferred to be part of the Onverwacht Group. Numerous quartz-feldspathic anatectic veinlets, containing plagioclase and quartz, are observed parallel to amphibolite. Barton *et al.* (1983b) report the Rb-Sr whole rock isochron age of the Stolzburg pluton to be 3481±92 Ma, and this is inferred to approximate the age of the Theeboom Cell.

Other samples: Several Cenozoic to Mesozoic granite, volcanic pyroclastic, and pelitic
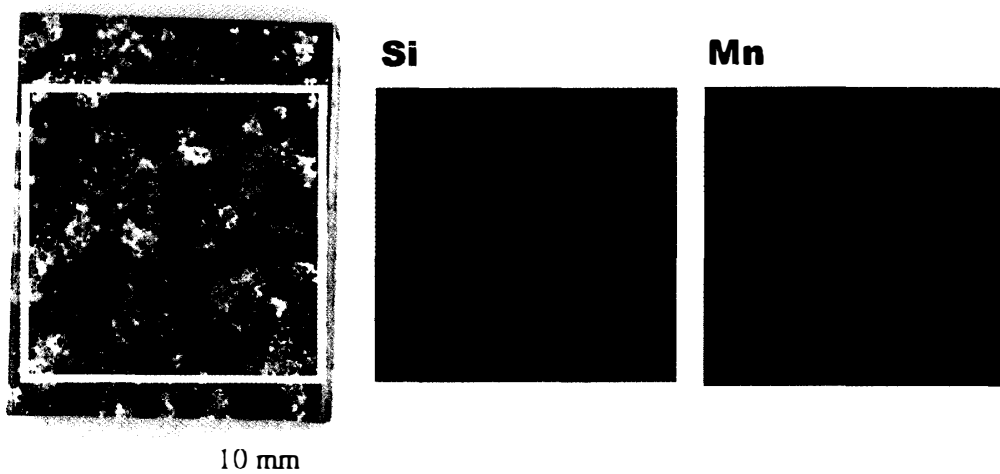
97082002B

Fig. 2.   Two-dimensional compositional maps for Si and Mn.

hornfels samples from Japan were examined, with results compared to data for Archean and Proterozoic rocks from South Africa. The petrochemical and geochronological characteristics of the respective Japanese rocks were described in Hareyama *et al.* (2000).

3. Experimental details

The imaging plate is a plate-like radiation sensor, and an effective means of obtaining images of two-dimensional natural radioactivity. The imaging plate method to determine the autoradiography for common rocks has been described by Hareyama *et al.* (2000).

Polished slab samples of minimum 10 mm thickness and 5×5 cm^2 area were laid on the imaging plate, inside of a shield box made of 'radioactive-free' iron. An absorber method was used, in order to discriminate alpha particles from other forms of radiation, since the alpha particles are most readily identified. Aluminum foil, 45 μm thickness, was placed on the surface of the imaging plate to shield most of the alpha particles. Two sets of irradiation experimental data were obtained, one with and another without the absorber, so that radiation images including and excluding alpha-ray radiation could be obtained. The exposure duration in air for the slab sample, at room temperature, was 72 hours.

The imaging plate mapping produces a digital image of PSL values, where a PSL value expresses the intensity of photostimulated luminescence in arbitrary units. PSL is proportional to the radioactivity and exposure duration, but strongly depends on the type of nuclides and quality of radiation (Fujifilm, 1993). In this study, One hundred PSL per mm^2 [arbitrary units/mm^2], was defined as the photostimulated luminescence intensity of the imaging plate after X-ray exposure from a W target (80 kV, 0.15 mR). The average PSL value per square mm was obtained from the whole polished surface area. Compositional mapping of the polished surface of selected rocks was determined by X-ray analytical microscope (XGT-2000, Horiba Ltd.) (Fig. 2). The experimental conditions are as follows: diameter of X-ray guide tube 100μm, 512×512 pixels for a given area, acquiring 1200 s per unit frame, and the integration quantity by $\times 200$.

4. Results and discussion

Results of XRF analyses of whole-rock major element composition and Zr concentration for 10 South African rock samples, as well as PSL values with and without an aluminum absorber, are presented in Table 1. Figure 3 shows examples of natural radioactivity mapping of slabs (97080806B, 97080703A-1, 97082002A, and 97081509B). Compositional maps for K and Si of the sample 97080806B are also shown in Fig. 3a. The measurement of natural radioactivity, using the imaging plate, was undertaken without the aluminum absorber. The distribution of radioactive sources within the rock is heterogeneous, with some high spots conspicuous in the 97080806B sample. Fig. 3a indicates that red areas in the radiation image correspond to the distribution of potassium. Thus, the bright or red areas on autoradiographs, which are indicative of high PSL value, mainly coincide with the occurrence of alkali feldspar. A few distinctive PSL spots are noted in 97080806B, whose high PSL spots were not observed by imaging plate mapping

N. Tsuchiya and M. Hareyama

Table 1.   Whole rock chemical composition and PSL values obtained by the imaging plate.

Serial No.	1	2	3	4	5	6	7	8	9	10
Sample No.	97080703A-1	97080806B	97081509A	97081509B	97082002A	97082002B	97082002C	97082002D	97082002E	97082103A-1
Rock Type	charnockite	Rapakivi granite	granite	charnockite	dunite	dunite	dunite	dunite	dunite	trondjhemitic gneiss
Geological Unit	NB	NB	SMZ-LB	SMZ-LB	JSB-BGB	JSB-BGB	JSB-BGB	JSB-BGB	JSB-BGB	TT-BGB
[wt%]										
SiO_2	60.31	70.45	68.95	58.50	35.18	36.85	37.66	40.38	37.32	73.22
TiO_2	1.73	0.49	0.81	2.03	0.02	0.02	0.02	0.02	0.02	0.25
Al_2O_3	14.85	14.57	14.05	13.81	0.47	0.04	0.16	0.38	0.15	15.44
Fe_2O_3	9.36	3.77	4.20	8.98	7.11	6.10	6.26	9.01	6.52	1.58
MnO	0.11	0.05	0.05	0.11	0.11	0.07	0.07	0.07	0.07	0.02
MgO	1.83	0.59	1.15	2.46	45.11	41.77	42.71	39.62	42.43	0.47
CaO	4.91	2.60	2.47	5.20	0.10	0.06	0.05	0.05	0.06	2.22
Na_2O	3.20	3.62	3.83	3.86	0.00	0.00	0.00	0.00	0.00	5.56
K_2O	3.09	3.78	3.91	2.29	0.00	0.01	0.01	0.01	0.01	1.57
P_2O_5	0.61	0.09	0.24	0.88	0.00	0.00	0.00	0.00	0.00	0.04
H_2O										
total	100.00	100.00	99.66	98.11	88.11	84.91	86.93	89.54	86.58	100.37
Zr (ppm)	701	396	364	557	2	3	4	4	3	128
[a.u./mm2]										
PSL without Al*	4.37	4.89	5.05	2.77	0.74	0.76	0.74	0.76	0.73	2.33
PSL with Al**	1.34	1.14	5.02	0.62	0.36	0.34	0.34	0.35	0.26	0.63

* measured without Al absorber

** measured with Al absorber interpolated between sample and IP

NB: The Natal Belt

SMZ-LB: Southern Marginal Zone of the Limpopo Belt

JSB-BGB: Jamestown Shist Belt in the Barberton Greenstone Belt

TT-BGB: Tonalite-Trondjhemite pluton in the Barberton Greenstone Belt
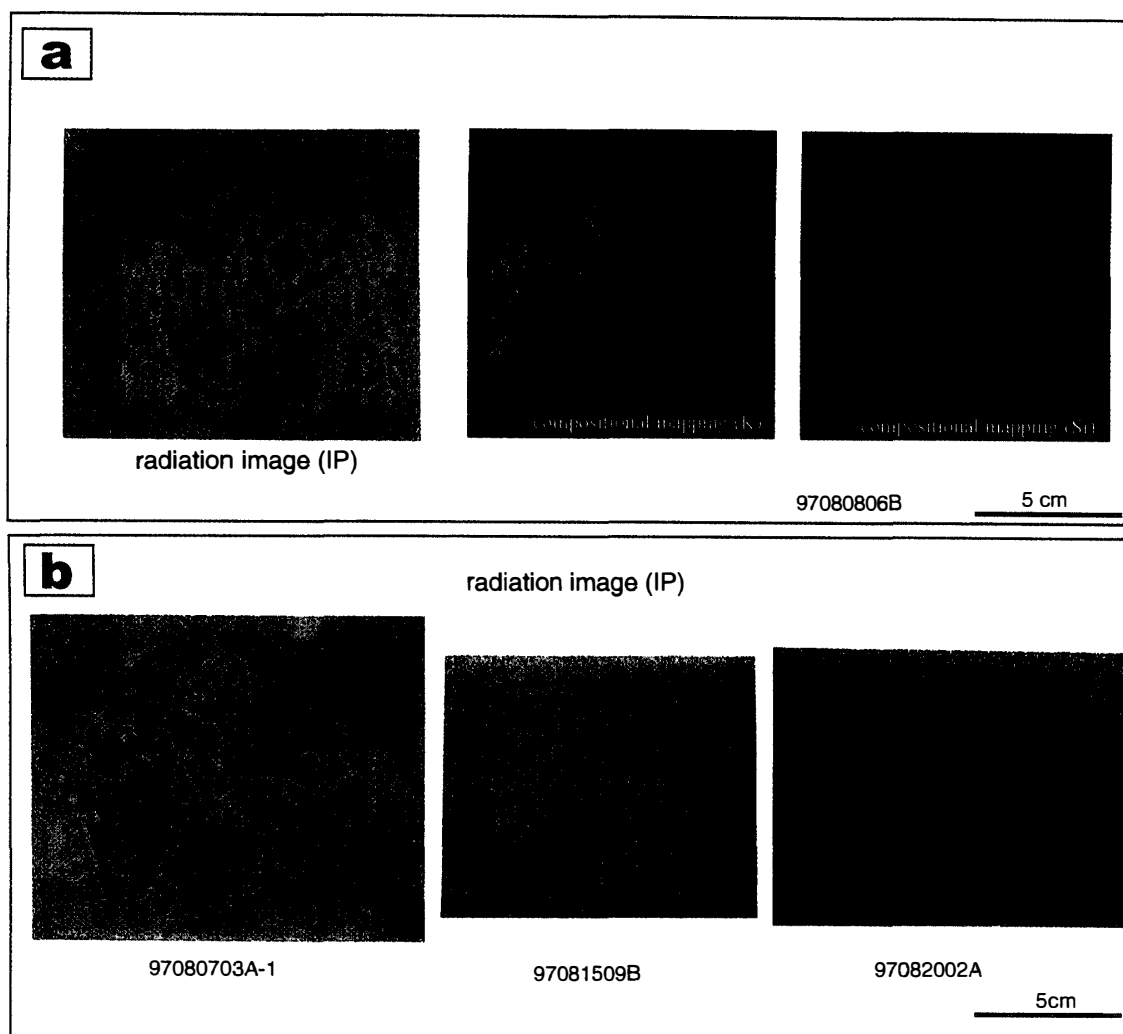
Fig. 3.   Examples of autoradiographs using the Imaging Plate without the aluminum Absorber ((a)
& (b)), and compositional maps for K and Si of the sample 97080806B (a).

with the aluminum absorber. We suggest that these distinctive PSL are alpha emitters,
and that they are likely to have been produced by highly radioactive rock-forming
minerals of mainly zircon and allanite.

Figure 4 shows the relationship between K_2O content and PSL value obtained for
experimental analysis conducted without the aluminum absorber. PSL value is
represented as an arbitrary quantity per unit area. Here, PSL value per square mm was
obtained from the entire polished surface area, including distinctive spots. PSL values are
shown to increase with increasing potassium content for all types of rocks analyzed,
including samples from both South Africa and Japan.

However, PSL values of the samples collected from South Africa, analyzed with the
aluminum absorber, were extremely low, as shown in Fig. 5. The aluminum foil inserted
between the rock and imaging plate absorbed emitted alpha particles, so the PSL map
shows only effects attributed to gamma and beta radiation. These observations suggest
that the natural radioactivity of the South African samples is not only controlled by the
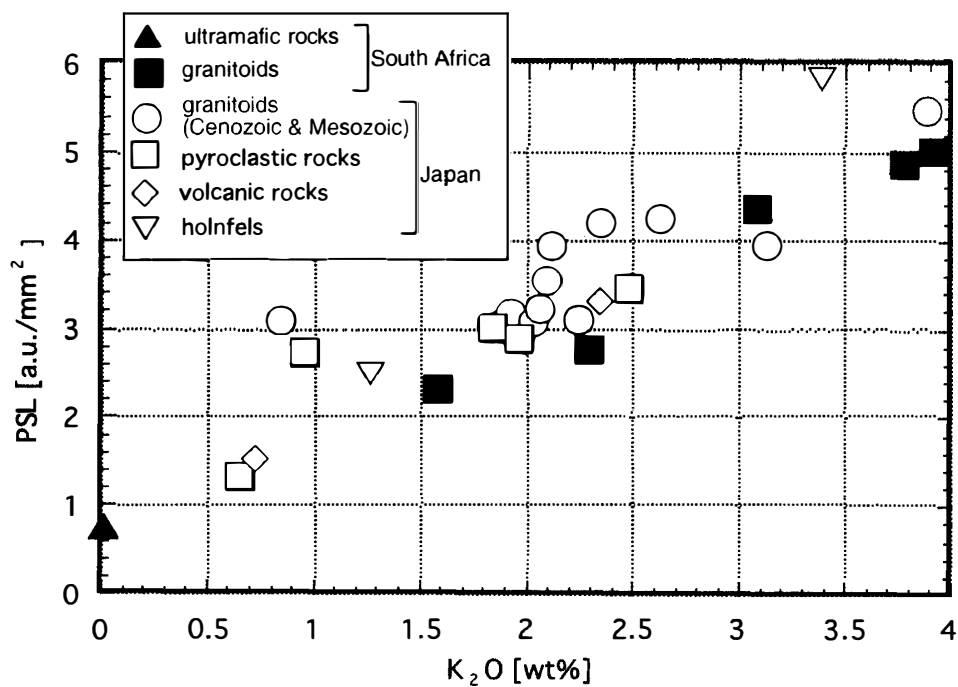
Fig. 4.   Relationship between K_2O content and PSL value. Measurement condition of
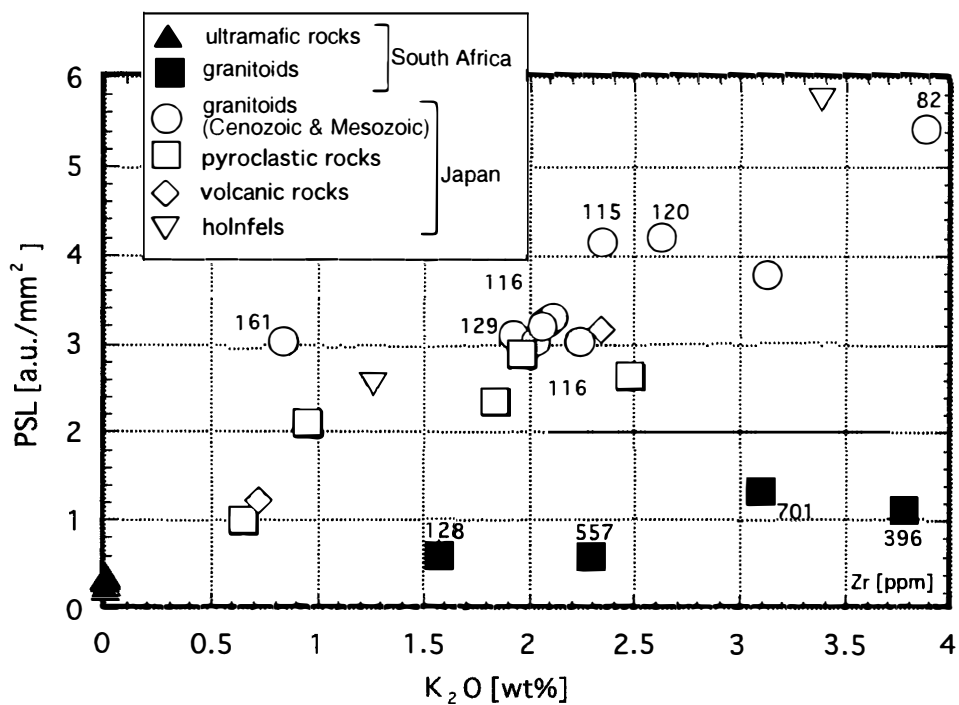the imaging plate is without the aluminum absorber.

Fig. 5.   Relationship between K_2O content and PSL value. Measurement condition of
the imaging plate is with aluminum absorber. The numbers with solid and
open squares (granitoids) indicate zirconium content in ppm.

beta and gamma dose from potassium, but also other radioactive sources. In other words, the linear correlation between potassium content and PSL in Fig. 4 is an apparent relationship, and the natural radioactivity of the Archean and Proterozoic samples actually depends on an additional alpha-emitter such as zircon and allanite. The effect of the alpha-emitter, as indicated by the zirconium content, is greater in the South African samples than in the Japanese granitoids analyzed in this study.

The range of alpha particles in most rocks is less than 0.1 mm despite a relatively long range for gamma rays. Measurable alpha rays are restricted to alpha emitters that appear on the surface of the slab sample. Consequently, a high whole rock zirconium content is not the direct cause of enhanced alpha ray radioactivity, but the relative area of the radioactive minerals exposed on the surface. For example, samples of 97080703A-1 (Zr: 701 ppm) and 97080806B (Zr: 396 ppm) with similar PSL values have different zirconium contents.

The major radioactive nuclides for effecting natural radioactivity of rocks include potassium (^{40}K), rubidium (^{87}Rb) , thorium (^{232}Th) and uranium (^{238}U, ^{235}U). The gamma-ray energy of ^{40}K is 1.46 MeV, which is relatively greater than that for gamma-ray peaks produced by the decay of thorium nuclides, or the ^{238}U and ^{235}U decay series, except for ^{214}Bi (^{238}U series) (Wordel et $al.$ 1994). For rocks analyzed in this study, whole rock potassium content is considerably larger than that of other radioactive nuclides, and consequently the disintegration of ^{40}K (and its high energy levels) is likely to have the greatest effect on natural beta and gamma-ray radioactivity. However, the quantities and energy dependence of radiation with respect to PSL value have not been established, thus, the PSL value indicates semi-quantitative units of dose. Further study is required to distinguish beta and gamma rays from alpha rays for evaluating true beta and gamma doses. Radioactive isotopic composition has to be measured precisely by high resolution radiation detectors such as HPGe gamma-ray spectroscopy under low background condition.

5. Conclusions

Two-dimensional radiation images of several kinds of rocks were obtained using a new highly-sensitive radiation detector. The imaging plate has the potential to be an effective research tool to evaluate two-dimensional natural radioactivity in rocks and other materials, due to its easy use and high sensitivity.

A semi-quantitative dose of natural radioactivity, represented by PSL value (the intensity of photostimulated luminescence per unit area), depends on whole rock chemical composition, particularly potassium content. In many cases, knowledge of whole rock potassium content is sufficient for approximate estimation of beta and gamma radiation. However, South African granitoids studied in this study, having high zirconium content compared to Japanese granitoids, indicate great radiation effects by disintegration of uranium, thorium and actinium decay series.

Acknowledgments

Japan–South Africa joint research program. The author also wishes to acknowledge Prof. D.D. van Reenen (Dept. Geology, Rand Afrikaans University), Mr. J.A.C. Jankowitz (Noble Peak Resources Ltd.), and Mr. Roelf le Roux (Barberton Mines Ltd.) for their helpful support during field work in the Barberton and Limpopo areas in South Africa. Thanks also due to Dr. Greg Bignall (Dept. Geoscience and Technology, Tohoku University) for valuable discussion. This study was financially supported by Grant-in-Aid for International Scientific Research No. 09041116 (Project Leader: Prof. K. Shiraishi, National Institute of Polar Research).

References

Anhaeusser, C.R. (1972): The geology of the Jamestown Hills area of the Barberton Mountain Land, South Africa. Trans. Geol. Soc. S. Afr., **75**, 225–263.

Anhaeusser, C.R., Robb, L.J. and Viljaen, M.J. (1983): Notes on the provisional geological maps of the Barberton Greenstone Belt and surrounding granitic terrane, Eastern Transvaal and Swaziland (1 : 250000 colour map). Spec. Publ. Geol. Soc. S. Afr., **9**, 221–223.

Grantham, G.H. and Eglington, B.M. (1992): Mineralogy, chemistry and age of granitic veins at Nicholson's Point, South Coast, Natal. S. Afr. J. Geol., **95**, 88–93.

Barton, J.M., Jr., Dutoit, M.C., Van Reenen, D.D. and Ryan, B. (1983a): Geochronologic studies in the Southern Marginal Zone of the Limpopo Mobile Belt, South Africa. Spec. Publ. Geol. Soc. S. Afr., **8**, 55–63.

Barton, J.M., Jr., Robb, L.J., Anhaeusser, C.R. and Van Nierop, D.A. (1983b): Geochronologic and Sr-isotopic studies of certain units in the Barberton granite-greenstone terrane, South Africa. Spec. Publ. Geol. Soc. S. Afr., **9**, 63–72.

Fujifilm Co., Ltd. (1993): BAS Technical Information, No. 1, 1–4.

Hareyama, M., Tsuchiya, N. and Takebe, M. (1998): Two-dimensional measurement of natural radioactivity of rocks by photostimulated luminescence. Proc. 9th Int. Symp. Water-Rock Inter., 835–838.

Hareyama, M., Tsuchiya, N., Takebe, M. and Chida, T. (2000): Two-dimensional measurement of natural radioactivity of granitic rocks by photostimulated luminescence technique. Geochem. J., **34**, 1–9.

Iwabuchi, Y., Mori, N., Takahashi, K., Matsuda, T. and Shinoya, S. (1994): Mechanism of photostimulated luminescence process in $BaFBr:Eu^{2+}$ phosphors. Jpn. J. Appl. Phys., **33**, 178–185.

McCourt, S. (1986): Archaean litologies in the Koedoesrand area, Northwest Transvaal. Spec. Publ. Geol. Soc. S. Afr., **8**, 113–119.

Momoshima, N., Sugihara, S., Shinno, I., Nita, J., Maeda, Y., Matsuoka, N. and Huang, C-H. (1995): Radioactive distribution in hokutolite from Hokuto hot spring, Taiwan measured with an imaging analyzer. Radioisotope, **44**, 389–394 (in Japanese with English abstract).

Robb, L.J. and Anhaesser, C.R. (1983): Chemical and petrogenic characteristics of Archean tonalite - trondhjemite gneiss plutons in the Barberton Mountain Land. Spec. Publ. Geol. Soc. S. Afr., **9**, 103–116.

Roering, C., Van Reenen, D.D., De Wit, M. J., Snit, C.A., De Beer, J.H. and Van Schalwyk, J.F. (1992): Structural geological and metamorphic significance of the Kaapvaal Craton - Limpopo Belt contact. Precambrian Res., **55**, 69–80.

Takahashi, K., Kohda, K., Miyahara, J., Kanemitsu, Y., Amitani, K. and Shionoya, S. (1984): Mechanism of photostimulated luminescence in $BaFBr:Eu^{2+}$ (X=Cl, Br) phosphors. J. Lumi., **31&32**, 266–268.

Takebe, M. and Abe, K. (1994): A novel particle identification with an imaging plate. Nucl. Inst. Meth., **A345**, 606–608.

Takebe, M., Abe, K., Souda, M., Satoh, Y. and Kondo, Y. (1995): A particle energy determination with an imaging plate. Nucl. Inst. Meth., **A359**, 625–627.

Thomas, M., Von Seggern, H. and Winnacker, A. (1991): Spatial correlation and photostimulability of defect centers in the X-ray-storage phosphor BaFBr:Eu^{2+}. Phys. Rev., **B44**, 9240–9247.

Tsuchiya, N., Hareyama, M. and Takebe, M. (1998): Measurement of natural radioactivity of rocks using imaging plate and its geological application. KEK- Proc., **98-4**, 313–322.

Van Reenen, D.D., Barton, J.M., Jr., Roering, C., Smit, C.A. and Van Schalkwyk, J.F. (1987): Deep crustal response to continental collision: the Limpopo belt of South Africa. Geology, **15**, 11–14.

Watkeys, M.K. (1983): Brief explanatory notes on the provisional geological map of the Limpopo Belt. Spec. Publ. Geol. Soc. S. Afr., **8**, 5–8.

Windley, B.F. (1996): The Evolution of Continents, 3rd ed. J. Wiley, 345–376.

Wordel, R., Mouchel, D., Solé, V.A., Hoogewerff, J. and Hertogen, J. (1994): Investigation of the natural radioactivity of volcanic rock samples using a low background gamma-ray spectrometer. Nucl. Inst. Meth., **A339**, 322–328.